THE EUROPEAN
PHYSICAL JOURNAL B

Regular Article

Influence of unlike dispersive interactions on methane adsorption in graphite: a grand canonical Monte Carlo simulation and classical density functional theory study

Matthew Lasich[a] and Deresh Ramjugernath

Thermodynamics Research Unit, School of Engineering, University of KwaZulu-Natal, Mazisi Kunene Road,
4041 Durban, South Africa

Abstract. Activated carbons are popular adsorbents due to their large micro- and mesoporous volumes and high specific surface areas. Modeling adsorption behaviour using molecular computations is frequently undertaken, but the influence of the unlike intermolecular interactions on adsorption behaviour is often not well understood. This study employed grand canonical Monte Carlo simulations, and classical density functional theory coupled with a simple lattice gas model to study the influence of unlike intermolecular interactions on adsorption behaviour, with a focus on the dispersive interactions. Both approaches yielded qualitative agreement with experimental data from the literature, although only a fitted classical density functional theory approach agreed quantitatively. Changing the potential energy well depth of the methane-carbon interaction did not change the Langmuir-type adsorption behaviour observed, however, there was some dependence of the adsorption behaviour on the unlike interactions, depending on the thermodynamic conditions.

1 Introduction

Activated carbon is a carbonaceous material containing numerous nanopores and is a popular adsorbent in industry and research. This is due to its large micro- and mesopore volumes, as well a high surface area to mass ratio [1]. In addition, sorption behavior of methane in carbon nanoporous materials is of interest in energy storage [2–7], and carbon sequestration in methane-containing coals [8–10]. Investigation of the physicochemical properties which influence adsorption and desorption can provide information for future energy research, carbon sequestration techniques, and the development of natural gas extraction methods. Computational methods may not only be used to interpret experimental results, but also to yield insights into the mechanisms themselves [11–13].

Pores in activated carbon are often described in terms of a slit pore [1,14–18]. This idealized structure provides a means to connect complex porosity and transport properties in carbon molecular sieves [19]. Previously, simulations have been performed to study methane in slit and slit-like carbon pores [8,20–22], although the influence of unlike interactions between methane and the carbon molecules constituting the pore walls has never been investigated in detail. The unlike interactions have been adjusted to fit to experimental datasets [21,23], however their effect on sorption behavior and mechanisms was not

studied. Classical density functional theory (CDFT) using simplified molecular models and mean field theory (the lattice gas employed in the present study is an example of a simplified molecular model) has also been employed previously to study adsorption in graphitic or carbonaceous pores [24,25]. However, as with molecular simulations, the influence of unlike interactions on adsorption behaviour has not been studied in detail.

The present study investigated the influence of the unlike dispersive interactions between methane and carbon on the adsorption behavior of methane in carbon nanopores, as represented by means of the slit pore model. This was undertaken using both self-consistent grand canonical Monte Carlo (GCMC) simulations, and mean field CDFT calculations employing a simple lattice gas. Previously, it was found that similar trends were found for the influence of unlike water-methane interactions on the thermodynamic behavior of methane clathrate hydrate [26–28] using a variety of methods. The similarity in trends may arise from the behavior of complex molecular systems being an emergent phenomenon. In other words, as long as the same force fields are employed, and the simulated species interact in a fundamentally similar manner, the net behavior of the system as a whole should remain the same, regardless of the computational technique employed. Therefore, it can be expected that both GCMC and CDFT calculations may yield similar trends in sorption behavior.

---

[a] e-mail: lasichm@ukzn.ac.za

Table 1. Intermolecular parameters used in this study.

Species	$\varepsilon_{ii}/\text{K}$	σ_{ii}/nm
Methane	148.1	0.381
Carbon	28.0	0.340

2 Theory and methods

2.1 GCMC simulations

The methane molecules were represented by a single Lennard-Jones (LJ) site [29–32], as were the individual carbon atoms [8]. This methane model provides a good approximation for the somewhat spherical methane molecule [33]. The intermolecular interactions are thus described by the following relationship:

$$U_{ij} = 4\varepsilon_{ij} \left[(\sigma_{ij}/r_{ij})^{12} - (\sigma_{ij}/r_{ij})^6 \right], \qquad (1)$$

where U_{ij} is the potential energy between site pairs i and j, ε_{ij} is the LJ potential energy well depth, σ_{ij} is the distance between sites i and j at which U_{ij} is zero, and r_{ij} is the intermolecular separation between sites i and j. In the GCMC simulations, intermolecular interactions were described using the LJ potential only, since methane and the graphitic slit pore walls have negligible electrostatic charges. For computational expediency, a cut-off radius of 1 nm was used for the LJ potential. The interactions between the methane molecules and the graphite pore walls were often described using the so-called 10-4-3 Steel potential [34] available in the literature, although for the sake of rigour in the GCMC simulations, this was not employed here. The intermolecular LJ parameters used in the GCMC simulations are listed in Table 1.

GCMC simulations employ the grand canonical ensemble [35], in which the chemical potential (μ), volume (V), and temperature (T) are held constant. These simulations mimic the adsorption/desorption of gas molecules into a confined space by considering creation/destruction Monte Carlo (MC) moves, respectively. The thermal motion of methane gas molecules was mimicked by means of translational moves. All of these MC moves were applied using the Metropolis scheme [36]. The probability of performing creation, destruction moves, or translation moves was set to 33.3% each. It may be noted that since methane was represented by a single LJ site, the spatial orientation of the inserted methane molecules was irrelevant. Since the carbon pore itself was a fixed structure, no MC moves were applied to the graphite sheets. In total, 1×10^7 MC moves were applied to the system, with the initial 2.5×10^6 moves (i.e., the first 25% of MC moves) being used to equilibrate the system, and the remainder to produce data. The GCMC simulations were performed using version 4.0.3 of the General Utility Lattice Program [37].

The carbon pore was described as lying between six graphite sheets (three above, three below). The gap between the two sets of carbon sheets (i.e., the carbon nanopore itself) was set to 1.4 nm, similar to a previous study [8]. The graphite sheets themselves were squares
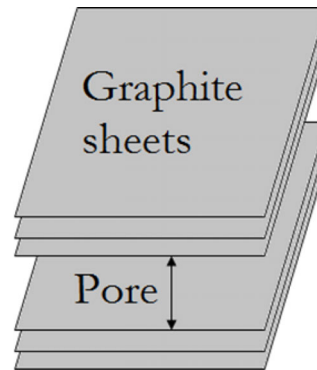
Fig. 1. Schematic diagram of the graphite slit pore used in the GCMC simulations.

of 2.2 nm × 2.2 nm, giving a total of about 552 carbon atoms per graphite sheet. This setup is illustrated in Figure 1.

For GCMC simulations, μ of the gas reservoir is required as an input. A computationally expedient approach is to calculate the value of μ using an equation of state. However, in this study, the gas phase was simulated explicitly by MC simulations in the isobaric-isothermal (NPT) ensemble using the ms-2 computer program [38]. This ensured that the GCMC simulations were self-consistent since exactly the same molecular force fields would be employed in Metropolis-type schemes [36] for both the gaseous and solid/adsorbed phases. This self-consistency can mitigate the effects of computational artifacts on any observed behaviour in the systems under investigation. For these simulations, 500 gas particles were used. Pre-equilibration relaxation consisted of 5×10^4 MC moves, followed by 1×10^7 canonical ensemble (NVT) steps, and 2.5×10^7 NPT moves for equilibrium. Production consisted of a further 2.5×10^8 MC moves. The chemical potential was estimated during the production stage of these simulations by means of Widom's method [39], using 2000 test particles. The results of these simulations are shown in Figure 2.

2.2 CDFT calculations

For the CDFT calculations, the confined gas species was considered as a square lattice gas exposed to an external field, with interactions between nearest-neighbours only. The density functional theory can actually be rather accurate for some simple pair-potential fluid interactions [40]. The model used in the CDFT calculations in the present study is simplistic, although it is computationally expedient as a result. This simplicity may not necessarily be a major disadvantage, since the aim of this study is not to produce quantitatively accurate adsorption isotherms, but to study the influence, if any, of unlike solid-fluid intermolecular interactions on the adsorption behaviour of methane on graphite. Therefore, provided the CDFT calculations and GCMC simulations produce qualitatively similar adsorption isotherm behaviour to experiments, the fundamental behaviour of these simulated systems should
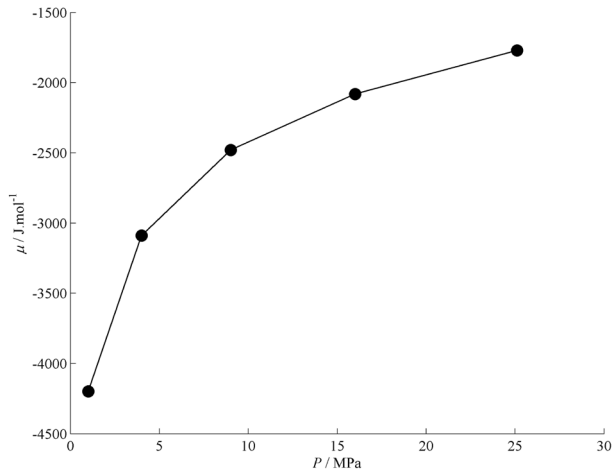
Fig. 2. Plot of chemical potential (μ) versus system pressure (P) for gaseous methane at $T = 300$ K, determined from MC simulations. Note that standard deviations for both P and μ were smaller than the symbols. The lines connecting points serve as a guide for the eye.

Fig. 3. Schematic diagram of the confined lattice gas model used in the CDFT calculations. Note that nearest-neighbour sites are those lying vertically or horizontally adjacent; not diagonally.

be satisfactory. The Hamiltonian (H) of any given state for this adsorbed lattice gas is given by [41–47]:

$$H = -0.5\varepsilon_{FF}\Sigma_i\Sigma_a(n_i n_{i+a}) + \Sigma_i(n_i\phi_i), \quad (2)$$

where ε_{FF} is the strength of nearest-neighbour interactions between gas molecules, n_i is the occupancy at site i, a is the vector from any given site to any other site which is a nearest-neighbour within the lattice, and ϕ_i is the external field describing the solid-fluid interactions between nearest-neighbours. For the present study, the carbon nanopore was considered as an infinite pore sandwiched between graphite sheets, and so the problem becomes one-dimensional. Figure 3 illustrates the lattice gas problem at hand.

Generally, CDFT involves the minimization of the grand free energy functional (Ω) with respect to number density (ρ). In this study, the mean field approximation was employed, which results in the following expression for Ω [48]:

$$\Omega(\{\rho_i\}) = kT\Sigma_i[\rho_i\ln\rho_i + (1 - \rho_i)\ln(1 - \rho_i)$$
$$- 0.5\varepsilon_{FF}\Sigma_i\Sigma_a(\rho_i\rho_{i+a}) + \Sigma_i\rho_i(\phi_i - \mu), \quad (3)$$

where ρ is the number density of site i, k is Boltzmann's constant, T is the temperature, and μ is the chemical potential of the adsorbed gas. It should be noted that ρ must lie between zero and one, and μ of the adsorbed gas is the same as for the gas in the reservoir supplying the adsorbed molecules. The set $\{\rho_i\}$ which results in a minimum for equation (2) represents the equilibrium distribution of gas molecules within the slit pore. The necessary conditions for the minimization of equation (2) are:

$$(\partial\Omega/\partial\rho_i)_{T,\mu} = 0 \quad \text{for all} \quad i. \quad (4)$$

Combination of equations (2) and (3) yield the following relationship which can be solved iteratively to determine the equilibrium distribution $\{\rho_i\}$ [49]:

$$kT\ln[\rho_i/(1 - \rho_i)] - \varepsilon_{FF}\Sigma_a\rho_{i+a} + \phi_i - \mu = 0 \text{ for all } i. \quad (5)$$

The equation above was solved iteratively until the absolute difference between iterations was within a tolerance of 10^{-6}.

The chemical potential of the bulk gas in the CDFT calculations was estimated by using an ideal gas approximation, with an adjustment for the lattice gas description [49]:

$$\mu = kT\ln(P) - kT\ln(kT/\Lambda^3) + 3kT\ln(\Delta r/\Lambda) \quad (6)$$

where P is the bulk pressure, Λ is the thermal de Broglie wavelength, and Δr is the separation between adjacent lattice sites, which in this case was set to σ_{FF}.

In the CDFT calculations, the intermolecular interactions between gas molecules and the pore wall, and amongst gas molecules, were approximated according to a square-well potential. Occupancy of sites closer than a minimum fluid-fluid separation, σ_{FF}, was disallowed (since this was the spacing between adjacent lattice sites), and the minimum separation between gas molecules and the solid surface was set to σ_{SF}. This incorporated repulsive effects between particles that approach too closely. The fluid-fluid parameters were set to the LJ values for the gas (see Tab. 1).

In the CDFT calculations, the solid-fluid energy term was calculated by assuming an average distribution of solid sites spread across the surface, with each site itself behaving like LJ carbon (see Tab. 1). In order to determine the number of interaction sites, and considering nearest-neighbour interaction only, the surface area considered was that bounded by a single lattice site, namely

a square of area σ_{FF}^2 centered at the projection of the nearest lattice site to the surface. This can be calculated as follows:

$$\phi_i = \varepsilon_{SF}\sigma_{FF}^2\rho_S, \qquad (7)$$

where ρ_S is the number density of interaction sites on the solid surface per unit area, which in this case was set to 114 nm^{-2} [34].

2.3 Unlike dispersive interactions

The unlike intermolecular interactions referred to in this study are the solid-fluid interactions between methane and carbon. In the GCMC simulations, intermolecular interactions were described in terms of the LJ potential, whereas the CDFT calculations considered a square-well type potential between nearest-neighbours. While these are naturally different intermolecular potentials, the main aim of this study was to examine the similarity in the adsorption behaviour between such different simulated systems, especially in comparison to available experimental data, with a focus on the influence of these unlike interactions. Previously for the methane-carbon system [21], the solid fluid interactions have been adjusted in an ad-hoc manner in order to more closely fit experimental data. This procedure has been used when studying water absorption in polymers [50], or even vapour-liquid-solid equilibria [51]. However, the behaviour of the simulated system that results from tweaking the unlike interactions has not been studied in great detail for many systems. Indeed, it has been shown that this simple fitting procedure can yield unexpected results such as phase dependence of the 'best fit' unlike energetic term [52], or an impossibility to fit to available experimental data within certain theoretical frameworks [28].

With regard to the present study, unlike intermolecular interactions for both the CDFT calculations and GCMC simulations were described using the popular Lorentz [53] and Berthelot [54] combining rules, respectively:

$$\sigma_{ij} = 0.5(\sigma_{ii} + \sigma_{jj}), \qquad (8)$$

$$\varepsilon_{ij} = (1 - k_{ij})(\varepsilon_{ii}\varepsilon_{jj})^{0.5}. \qquad (9)$$

The Berthelot rule described above in equation (9) is in fact a modified form of the original which incorporates a correction or adjustment factor k_{ij} which describes the strength of the unlike dispersive interaction ε_{ij} relative to the baseline scenario. The description above of the unlike dispersive interactions is presented from the perspective of force fields used in GCMC simulations. In the case of CDFT calculations, the unlike dispersive interaction is represented by ϕ_i; see equations (2), (3), (5), and especially (7).

The Berthelot rule itself is derived from a more generic formulation by Reed [55], and extended by Hudson and McCoubrey [56]:

$$\varepsilon_{ij} = [2(I_{ii}I_{jj})^{0.5}/(I_{ii} + I_{jj})]$$
$$\times [2(\sigma_{ii}\sigma_{jj})^{0.5}/(\sigma_{ii} + \sigma_{jj})](\varepsilon_{ii}\varepsilon_{jj})^{0.5}. \qquad (10)$$

The general formulation employs both the ionization potentials (I) and molecular size parameters to calculate ε_{ij}. In the case of these two properties being similar for the molecules under consideration, the Berthelot rule is returned. While there are indeed a great variety of combining rules in the literature, it should be noted that the total range of different ε_{ij} and σ_{ij} values may in fact not be very large. In a recent study on methane clathrate hydrate systems [57], ε_{ij} calculated from a wide array of combining rules did not deviate from the Berthelot-derived value by more than about eight percent, and σ_{ij} deviated no more than about one percent from the Lorentz-derived value. While the present system is not a clathrate hydrate system, the aforementioned system consisted of methane + water (i.e., a nonpolar molecule interacting with a highly polar species, respectively), and as the present system is methane + carbon, it can be expected that the deviations from the Lorentz-Berthelot baseline will not be large, if any number of different combining rules were used. Moreover, the Berthelot rule serves as a convenient baseline, since it is commonly used, and many researchers may be familiar with it. Since the various combining rules applied to the size term σ_{ij} do not produce significantly varying results, the effect of deviation from the Lorentz rule may not be of any practical or real physical interest.

With regard to previous studies which fitted the unlike interactions to available experimental data for the amount of gas adsorbed as a function of pressure, it should be noted that for the case of methane on carbon black at $T = 273$ K, the best match was obtained with $k_{ij} = 0.2$ [21], whereas for methane at $T = 113$ K, the appropriate value was $k_{ij} = -0.025$ [23]. This suggests that close to ambient conditions, the Berthelot rule significantly overestimates the unlike dispersive interactions, whilst at cryogenic temperatures, it produces a slight underestimate. This of course means that for any given system, several different values of k_{ij} may produce a best fit to experimental data, depending on the thermodynamic conditions, and that this binary correction factor may be positive or negative. Therefore, the influence of unlike intermolecular interactions on the adsorption behaviour of the simulated methane + carbon system is necessarily important, due to the possibility of best fit k_{ij} values producing both increases and decreases in ε_{ij}, relative to the Berthelot case.

3 Results and discussion

3.1 GCMC simulations

The results of the GCMC simulations for methane adsorbed in a graphitic slit pore of width 1.4 nm are shown in Figure 4. The quantity on the y-axis (q) is the amount of gas adsorbed into the nanoporous carbon material. The simulations were performed for a range of values of the unlike interaction parameter: $k_{ij} = \{-0.5, -0.1, 0.0, +0.1, +0.5\}$ (see Eq. (8)). The corresponding unlike interaction terms in this case are $\varepsilon_{ij} = \{96.6, 70.8, 64.4, 58.0, 32.2\}$ K. It is clear that the results
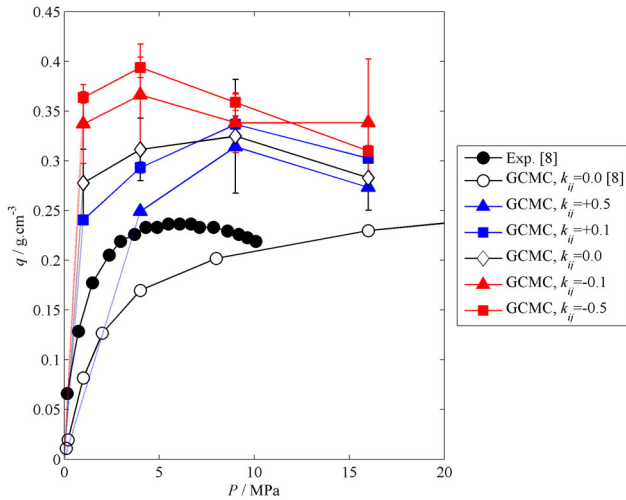
Fig. 4. Results of GCMC simulations of methane adsorption in a graphitic slit pore of width 1.4 nm compared to experimental data and previous simulations at $T = 300$ K. The lines connecting points serve as a guide for the eye. The error bars represent the standard deviations.

Fig. 5. Comparison of gas phase MC simulations with the ideal gas and experimental PVT data. Note that standard deviations for both P and ρ were smaller than the symbols. The lines connecting points serve as a guide for the eye.

of the GCMC simulations for the baseline scenario (i.e., $k_{ij} = 0.0$) do not agree with the results of the previous molecular simulations [8]. However, it must be noted that the GCMC simulations performed in the present study were self-consistent, in that the chemical potential of the methane gas reservoir was estimated as a function of pressure by means of single phase MC simulations, which was not the case in the previous study. Therefore, this discrepancy may arise as an artifact of the different descriptions used for the methane gas reservoir supplying the adsorbed methane molecules into the slit pore. In this regard, it is clear that the self-consistent simulations result in an overestimation of the amount of adsorbed methane as compared to the experiments, which is thus a result of the methane force field used, and not an artifact arising from inconsistencies in force field or computational technique used.

Below $P \approx 7$ MPa, decreasing k_{ij} results in an increase in the amount of methane adsorbed. This can be expected, since a decrease in k_{ij} necessarily produces an increase in the depth of the LJ potential energy well between methane and carbon, as ε_{ij} and k_{ij} are inversely related to one another (see Eq. (9)). Changing the unlike interaction does not appear to alter the adsorption behaviour of the simulated system in any significant way. Therefore, it is entirely feasible to adjust the unlike interactions in order to fit to experimental data, at low to moderate pressures.

At higher pressures (i.e. $P > 7$ MPa), however, there was no clear trend in terms of the adsorption isotherm behaviour as a function of the unlike dispersive interactions. This can be attributed to the gas-gas interactions playing an increasingly prominent role relative to the solid-fluid interactions. In this regard, however, it should be noted that this does not necessarily mean that on a molecule-

by-molecule basis the solid-fluid interactions are relatively weaker. Instead, at higher pressures there are simply more adsorbed methane molecules, and as an aggregate, the total cumulative strength of the fluid-fluid interactions may begin to play a larger role in adsorption behaviour.
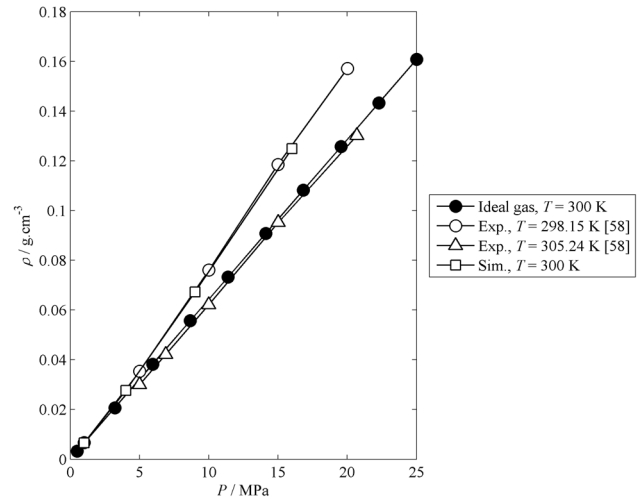
A potential source of deviation can be the behaviour of the pure methane gas, as represented by the force field in this study, as compared to real methane gas. In addition, the CDFT calculations in this work employ the ideal gas description of methane, which may contribute to deviations in behaviour compared to both experimental data and the results of the GCMC simulations. A comparison between the ideal gas, the results of the gas phase MC simulations, and experimental PVT data from the literature [58] are shown in Figure 5. In this case, it is apparent that the methane force field overestimates the gas phase density as compared to both reality and the ideal gas model. Therefore, in the self-consistent simulations at a given pressure, it can be expected that the methane may adsorb more than for a corresponding ideal gas or real gas at the same pressure. This may be a source of the difference observed in the present study with regard to the amount of gas adsorbed, since the self-consistent GCMC simulations yielded more adsorbed methane than the previous experimental or simulation work [8].

In addition to the adsorption isotherms, the spatial distribution of adsorbed methane molecules within the slit pore was analysed. This was achieved by sampling 10^3 configurations generated by the GCMC simulations, and generating histograms resulting from computing the distances between methane and carbon sites. The histograms could then be used to determine the radial pair distribution function $g(r)$ describing the location of methane molecules relative to carbon atoms in the slit pore. This can give an idea of not only the spatial distribution, but also the type of adsorption behaviour observed, since if the
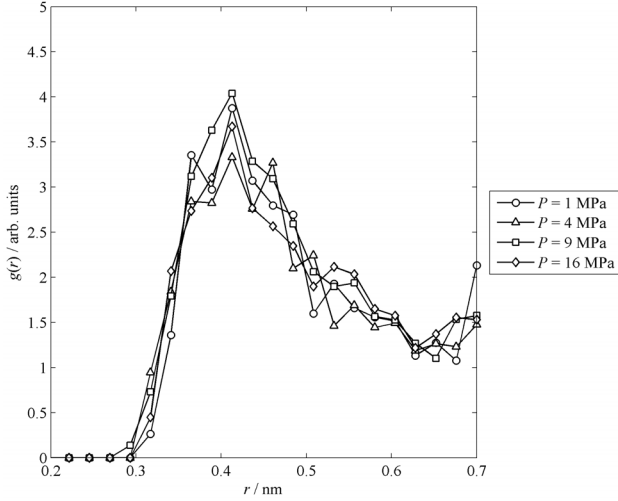
Fig. 6. Plot of the radial pair distribution function $g(r)$ for methane-carbon at $T = 300$ K, as a function of intermolecular separation r, for $k_{ij} = 0$.

Fig. 7. Plot of the radial pair distribution function $g(r)$ for methane-carbon at $T = 300$ K, as a function of intermolecular separation r, for $k_{ij} = \{+0.5, -0.5\}$. At $P = 1$ MPa, $r_{\max} \approx \{0.41, 0.41\}$ nm, and at $P = 16$ MPa, $r_{\max} \approx \{0.44, 0.37\}$ nm, respectively.

system conformed to monolayer Langmuir-type adsorption [59], the adsorbed methane molecules should necessarily be found in a monolayer alongside the pore wall. The results of these calculations are shown in Figure 6 for the baseline scenario (i.e., the Berthelot case). It can be noted here that the first peak in all cases (at $r \approx 0.41$ nm) lies close to the equilibrium distance for the methane-carbon Lennard-Jones spheres ($r = 2^{1/6}\sigma_{SF} = 0.4046$ nm).

It is instructive to examine the ratios of the peaks of $g(r)$, by comparing the value of the radial pair distribution function for the first peak (i.e., molecules lying adjacent to the surface, at a distance $r_{\max}$) with its value at $r = 0.7$ nm (since the pore is 1.4 nm wide). This ratio Π can be defined as follows:

$$\Pi \equiv g(r_{\max})/g(0.7 \text{ nm}). \tag{11}$$

For the Berthelot case, Figure 6 shows that with increasing pressure (from 1 MPa to 16 MPa at least), Π increases. In quantitative terms, the values of Π at $P = 1$ MPa and $P = 16$ MPa are 1.8 and 2.2, respectively (a relative difference of approximately 22%). In terms of the scale of this difference relative to uncertainties in the data shown in Figure 6, there was an estimated uncertainty in $g(r)$ of about 16% at $r_{\max}$ and about 12% at $r = 0.7$ nm. Therefore, the density difference shown in terms of Π may not be conclusive, and further study can be conducted in this area. This may indicate the filling of the monolayer adjacent to the pore wall, thus resembling Langmuir-type adsorption. The relevant values of q in this case are approximately 0.278 g cm^{-3} and 0.283 g cm^{-3}, respectively. In order to determine the effect of the unlike dispersive interactions on the adsorption behaviour, it is necessary to perform the same analysis presented in Figure 6 for different k_{ij} values. For comparative purposes, only the radial pair distribution functions are shown for $k_{ij} = +0.5$ and $k_{ij} = -0.5$ in Figure 7. In this case, increasing the magnitude of ε_{SF} (in other words, decreasing k_{ij}) results
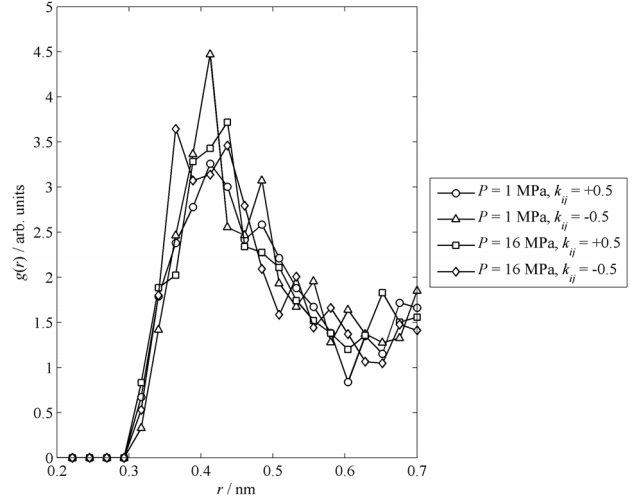
in a more pronounced difference in Π at high pressure as compared to low pressure. Numerically, the ratio of Π at $P = 16$ MPa as compared to $P = 1$ MPa is 1.6 for $k_{ij} = -0.5$, as compared to 0.8 for $k_{ij} = +0.5$. However, the adsorption isotherms shown in Figure 4 suggest that this relative difference in number density may be overcome by increases in the overall amount of methane adsorbed outside the monolayer, since there is little difference in the adsorption isotherms for each k_{ij} value at higher pressures. This suggests that the effect of changing the solid-fluid interactions may be more pronounced under certain thermodynamic conditions, in terms of the effect on the adsorbed monolayer. It can also be noted that the pressures investigated in the present study were not very high, in absolute terms, and given the trends shown for the simulated adsorption isotherms, it may be expected that at pressures far above $P = 16$ MPa, there may also be little difference between the results of simulations using different k_{ij} values.

3.2 CDFT calculations

For the CDFT calculations, several different approaches were considered. In addition to the methodology described in Section 2 above, fitting to the results of the GCMC simulations as well as available experimental data was also undertaken. Fitting in this case involved adjusting intermolecular parameters to better match the reference data, by means of a simplex method [60], with a tolerance of 10^{-6}. With regard to the intermolecular parameters that were considered for fitting, a modification to the Lorentz [53] combining rule needs to be introduced:

$$\sigma_{ij} = 0.5(1 - l_{ij})(\sigma_{ii} + \sigma_{jj}) \tag{12}$$

Table 2. Results from fitting the CDFT model to experimental data [8].

1-Parameter	
k_{ij}	+0.03
2-Parameter	
k_{ij}	+0.03
l_{ij}	−0.01
4-parameter	
k_{ij}	−0.28
l_{ij}	+0.29
$\varepsilon_{FF}/\mathrm{K}$	42.6
σ_{FF}/nm	0.331

Fig. 8. Results of CDFT calculations of methane adsorption in a graphitic slit pore of width 1.4 nm, fitted to experimental data at $T = 300$ K. Note that the 1-parameter calculation curve overlap almost entirely with 2-parameter calculation curve.

in which l_{ij} serves as a fitting parameter for the unlike size term. In effect, l_{ij} acts a means to adjust the closeness with which the adsorbed monolayer may lie in relation to the graphite pore walls. Thus, k_{ij} and l_{ij} together allow for the mitigation of any simplifications or assumptions which may affect the description of the solid-fluid intermolecular interactions. In addition to these unlike correction terms, the pure fluid parameters ε_{FF} and σ_{FF} were also considered for the purposes of fitting, to account for the fluid-fluid interactions in the confined space of the pore possibly being different to the case for the free fluid. Therefore, several different combinations of adjustable variables were used to fit to experimental data:

- k_{ij} only;
- k_{ij} and l_{ij};
- k_{ij}, l_{ij}, ε_{FF} and σ_{FF}.

In this way, the effects of any simplifying assumptions could be mitigated, and the simple lattice gas model could be 'calibrated' to available adsorption isotherm data.

The results of the parameter fitting using CDFT are shown in Table 2, and the associated adsorption isotherms are shown in Figure 8. It was clear that the calculated adsorption isotherm only agreed qualitatively with the experimental results [8], except for the case in which the effective fluid species properties were also fitted to the reference dataset. This suggests that the primary shortcoming of the CDFT approach used in this study was in the description of pure methane. Moreover, the results of the 1- and 2-parameter fitting are not significantly different, and the fitted values for k_{ij} and l_{ij} show that these could not be adjusted much to improve the fit; further emphasizing this point. Fitting the intermolecular parameters for pure methane as well as the correction factors for the combining rules yielded an agreeable fit to the experimental data, both qualitatively and quantitatively. The results of this fitting exercise also suggest that in order to adequately describe real systems, the pure fluid interaction parameters (i.e., the potential energy well depth and minimum intermolecular separation) for a square lattice gas with nearest-neighbour interactions may need to be significantly less than for a LJ gas. This may be especially the case for the potential energy well depth, which had to
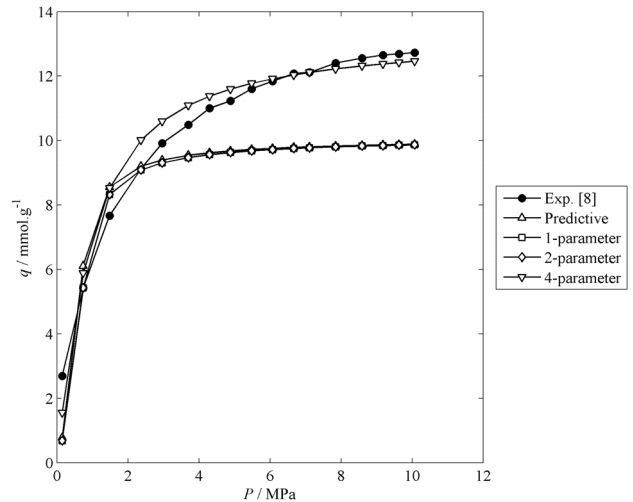
be reduced by a factor of about 3.5 in order to fit to the experimental data. This suggests that in the confined state, the methane-methane interactions are dampened by the presence of nearby carbon atoms, relative to the gaseous state. For comparison, the fitted value for σ_{FF} was a maximum of 14% different from the parameter used in the predictive calculation (see Tab. 1). It can be noted that adjusting l_{ij} and σ_{FF} together is essentially changing the distance between the adsorbed monolayer and the pore wall, and so the value of l_{ij} obtained by means of the 4-parameter fitting approach amounts to changing the value of σ_{SF}.

The results of the predictive CDFT calculations can also be considered in relation to the discrepancy between the ideal gas and the force field used to describe the methane gas in the GCMC simulations (see Fig. 5). As stated previously, the CDFT calculations in this study employed the ideal gas model to describe the methane gas. Comparison of the results shown above in Figure 8 with the results from the GCMC simulations shown in Figure 4 show that while the GCMC simulations produced an overestimate in terms of the amount of methane adsorbed, the predictive CDFT calculations result in an underestimate. This can be related to the density of the gas reservoir supplying the methane molecules for adsorption into the slit pore, since Figure 5 showed that the ideal gas model slightly underestimates the density of gaseous methane, while the methane force field produced an overestimate.

Once the simple lattice gas CDFT model was fitted to experimental data, an exploratory study could be undertaken, similar to that performed using GCMC simulations, in which the unlike intermolecular interactions were adjusted to study the adsorption behaviour of the methane + graphite system. In this exploratory study, only the unlike energy correction term k_{ij} was adjusted,
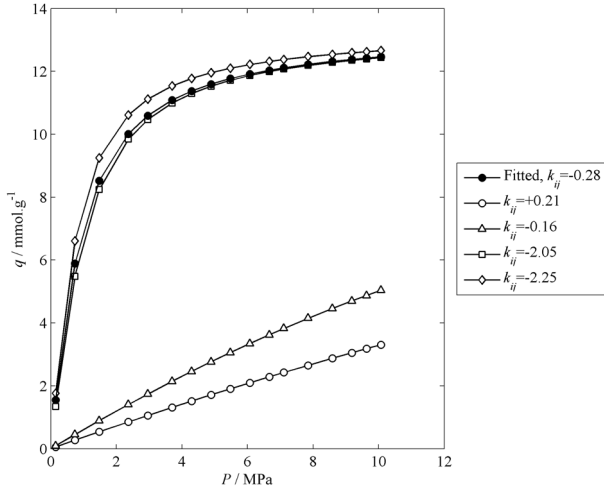
Fig. 9. Results of the exploratory CDFT calculations of methane adsorption in a graphitic slit pore of width 1.4 nm at $T = 300$ K, for selected values of k_{ij}.

Fig. 10. Density profiles resulting from the CDFT calculations. The lines connecting the values for each lattice point are guides for the eye. The apparent off-centered appearance is an artifact of the square lattice grid construction.

since this is most often adjusted to fit to experimental data, and as stated previously, fitting l_{ij} and σ_{FF} simultaneously to experimental data is analogous to changing σ_{SF}. The results of the exploratory calculations are shown in Figure 9, for a selected range of k_{ij} values.

It was apparent that increasing k_{ij} has little effect once the graphitic slit pore is already at high loading values, since relatively large increases in the magnitude of ε_{ij} (i.e., for $k_{ij} = -2.05$ and $k_{ij} = -2.25$) result in a marginal shift in the adsorption isotherm curve. This is especially the case at high pressure, which may be expected, since the slit pore is at or near its maximum capacity for adsorbed methane. Decreasing ε_{ij}, however, does result in a marked decrease in the amount of methane adsorbed into the graphitic pore. This can be expected, since a reduction in the strength of solid-fluid interactions may necessarily result in a reduced monolayer density within the pore. It can be noted that this reduction is more marked at high pressure, which may be due to the reduced strength of the solid-fluid interactions essentially extending the pressure range over which loading occurs. This behaviour may be significant in modeling gas adsorption in situations where the system pressure relative to the critical or saturation pressure is of interest.

As with the configurations generated by the GCMC simulations (see Figs. 6 and 7), the number density spatial distribution produced as a result of the CDFT calculations can be instructive. In this case, however, the density profile $\{\rho_i\}$ was determined directly in order to minimize the grand free energy functional by means of equation (5). The results of this procedure, in terms of the density profiles, are shown in Figure 10. It is clear that the density profiles are similar for the predictive calculations and the 1- and 2-parameter models. In these three cases, due to the lattice spacing afforded by σ_{FF} and the available free volume allowed by σ_{SF} in conjunction with the pore width of 1.4 nm, there is always only a monolayer formed. Each surface monolayer would in ef-

fect be adjacent to the monolayer on the opposite surface, due to the aforementioned spatial constraints. With the 4-parameter model, however, the fitted values for σ_{FF} and σ_{SF} are different, and allowed for the formation of two distinct monolayers. It is observed that, at least for the pressure range considered in this study, no pore filling outside the surface monolayers occurred. This strongly suggests Langmuir-type adsorption behaviour. Significantly, the values of ε_{SF} arising from each fitting procedure did not play a role in the number density of the adsorbed monolayer. The adsorption isotherms resulting from the exploratory CDFT calculations (see Fig. 9) also suggest that significantly increasing ε_{SF} may not alter the density profiles significantly, since there is little separating the adsorption isotherms for $k_{ij} = -0.28$ and $k_{ij} > -2$. However, in scenarios where ε_{SF} is noticeably reduced (as in Fig. 9), it can be expected that the monolayer density would be necessarily reduced as well.
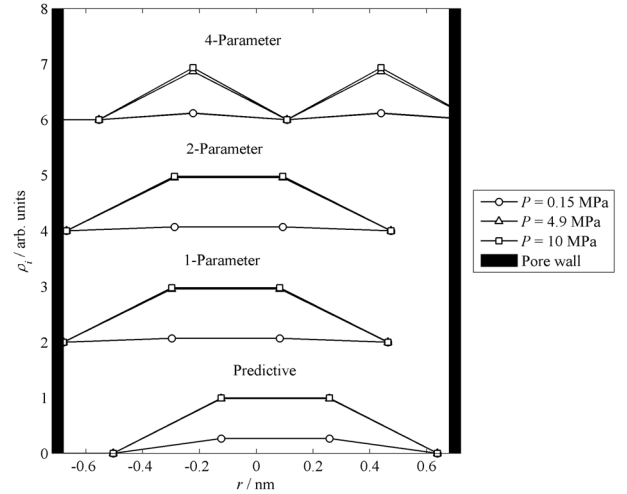
4 Conclusions

Self-consistent GCMC simulations and mean field lattice gas CDFT calculations were used to model adsorption of methane in graphitic slit pores, and study the effect, if any, of unlike intermolecular interactions on adsorption behaviour. The results of the GCMC simulations agreed qualitatively with experimental data taken from the literature [8], and for $P < 7$ MPa, there was a clear trend in terms of the amount of methane adsorbed versus the unlike dispersive energy ε_{SF}: decreasing the magnitude of the potential energy well depth ε_{SF} (i.e. increasing k_{ij}) reduced the amount of methane adsorbed into the slit pore. However, at higher pressures (i.e., $P > 7$ MPa), there was no discernable trend.

CDFT calculations were used to fit intermolecular parameters to the experimental data [8], according to various combinations of adjustable parameters:

– k_{ij} only;
– k_{ij} and l_{ij};
– k_{ij}, l_{ij}, ε_{FF} and σ_{FF}.

All models agreed qualitatively with the literature, although only the 4-parameter model produced a quantitatively agreeable fit. Exploratory calculations for various values of k_{ij} were undertaken for the 4-parameter CDFT model, and it was found that increasing the magnitude of the potential energy well depth ε_{SF} did not shift the adsorption isotherm curve significantly, although reducing it could change the methane loading noticeably. Examination of the density profiles resulting from the CDFT calculations showed that unless σ_{FF} and σ_{SF} were reduced, the monolayers on each pore wall would be adjacent, and practically indistinguishable. In addition, the pair distribution functions generated during the GCMC simulations showed density distributions that agreed more closely with the results from the 4-parameter CDFT calculation. This suggested that the square lattice gas description of methane adsorbed in graphite should have intermolecular overlap distances less than that for comparable LJ species.

Author contribution statement

ML designed the study with suggestions from DR. ML performed the calculations. ML wrote the manuscript with suggestions from DR.

References

1. A. Wongkoblap, D.D. Do, J. Colloid Interface Sci. **297**, 1 (2006)
2. D. Lozano-Castello, J. Alcaniz-Monge, M.A. de la Casa-Lillo, D. Cazorla-Amoros. A. Linares-Solano, Fuel **81**, 1777 (2002)
3. S. Biloe, V. Goetz, A. Guillot, Carbon **40**, 1295 (2002)
4. S. Jiang, J.A. Zollweg, K.E. Gubbins, J. Phys. Chem. B **98**, 5709 (1994)
5. V.C. Menon, S. Komarneni, J. Porous Mater. **5**, 43 (1998)
6. M. Eddaoudi, J. Kim, N. Rosi, D. Vodak, J. Wachter, M. O'Keeffe, O.M. Yaghi, Science **295**, 469 (2002)
7. J.L. Atwood, L.J. Barbour, A. Jerga, Science **296**, 2367 (2002)
8. P. Billemont, B. Coasne, G. De Weireld, Langmuir **27**, 1015 (2011)
9. C.M. White, D.H. Smith, K.L. Jones, A.L. Goodman, S.A. Jikich, R.B. La Count, S.B. Du Bose, E. Ozdemir, B.I. Morsi, K.T. Schroeder, Energy Fuels **19**, 659 (2005)
10. M. Mazzotti, R. Pini, G. Storti, J. Supercrit. Fluid. **47**, 619 (2009)
11. B. McEnaney, J. Mays, X. Chen, Fuel **77**, 557 (1998)
12. Z. Tan, K.E. Gubbins, J. Phys. Chem. B **94**, 6061 (1990)
13. *Fluid Interfacial Phenomena*, edited by C.A. Croxton (Wiley, Chichester, 1986)
14. R.F. Cracknell, D. Nicholson, N. Quirke, Phys. Rev. Lett. **74**, 2463 (1995)
15. O.G. Jepps, S.K. Bhatia, D.J. Searles, J. Chem. Phys. **120**, 5396 (2004)
16. Y.-I. Lim, S.K. Bhatia, T.X. Nguyen, D. Nicholson, J. Membr. Sci. **355**, 186 (2010)
17. D. Nicholson, Langmuir **15**, 2508 (1999)
18. D. Nicholson, Carbon **36**, 1511 (1998)
19. K.M. Steel, W.J. Koros, Carbon **43**, 1843 (2005)
20. V.Yu. Gusev, J.A. O'Brien, N.A. Seaton, Langmuir **13**, 2815 (1997)
21. P. Kowalczyk, H. Tanaka, K. Kaneko, A.P. Terzyk, D.D. Do, Langmuir **21**, 5639 (2005)
22. Y.-I. Lim, S.K. Bhatia, J. Membr. Sci. **369**, 319 (2011)
23. D.D. Do, H.D. Do, Fluid Phase Equilibr. **236**, 169 (2005)
24. M.B. Sweatman, N. Quirke, J. Phys. Chem. B **105**, 1403 (2001)
25. M.B. Sweatman, N. Quirke, Langmuir **18**, 10443 (2002)
26. M. Lasich, A.H. Mohammadi, K. Bolton, J. Vrabec, D. Ramjugernath, Phil. Mag. **94**, 974 (2014)
27. M. Lasich, A.H. Mohammadi, K. Bolton, J. Vrabec, D. Ramjugernath, Fluid. Phase Equilibr. **369**, 47 (2014)
28. M. Lasich, A.H. Mohammadi, K. Bolton, J. Vrabec, D. Ramjugernath, Fluid Phase Equilibr. **381**, 108 (2014)
29. M. Lasich, Ph.D. thesis, University of KwaZulu-Natal, 2014
30. J.E. Lennard-Jones, Proc. Phys. Soc. **43**, 461 (1931)
31. J.J. Potoff, A.Z. Panagiotopoulos, J. Chem. Phys. **109**, 10914 (1998)
32. J.M. Smith, H.C. Van Ness, M.M. Abbott, *Introduction to Chemical Engineering Thermodynamics*, 7th edn. (McGraw-Hill, New York, 2005)
33. A.M. Vieira-Linhares, N.A. Seaton, Chem. Eng. Sci. **58**, 4129 (2003)
34. W.A. Steele, Surf. Sci. **36**, 317 (1973)
35. G.E. Norman, V.S. Filinov, High Temperature **7**, 216 (1969)
36. N. Metropolis, A.W. Rosenbluth, M.N. Rosenbluth, A.H. Teller, E. Teller, J. Chem. Phys. **21**, 1087 (1953)
37. J.D. Gale, A.L. Rohl, Mol. Simulat. **29**, 291 (2003)
38. S. Deublein, B. Eckl, J. Stoll, S.V. Lishchuk, G. Guevara-Carrion, C.W. Glass, T. Merker, M. Bernreuther, H. Hasse, J. Vrabec, Comput. Phys. Commun. **182**, 2350 (2011)
39. B. Widom, J. Chem. Phys. **39**, 2808 (1963)
40. M.B. Sweatman, Phys. Rev. E **63**, 031102 (2001)
41. M.J. De Oliveira, R.B. Griffiths, Surf. Sci. **78**, 687 (1978)
42. C. Ebner, Phys. Rev. A **22**, 2776 (1980)
43. E. Bruno, U.B.M. Marconi, R. Evans, Physica A **141**, 187 (1987)
44. E. Kierlik, P.A. Monson, M.L. Rosinberg, L. Sarkisov, G. Tarjus, Phys. Rev. Lett. **87**, 055701 (2001)
45. H.J. Woo, P.A. Monson, Phys. Rev. E **67**, 041207 (2003)

46. C. Ebner, Phys. Rev. A **23**, 1925 (1981)
47. R. Pandit, M. Schick, M. Wortis, Phys. Rev. B **26**, 5112 (1982)
48. P.A. Monson, Langmuir **24**, 12295 (2008)
49. A. Valencia, M. Brinkmann, R. Lipowsky, Langmuir **17**, 3390 (2001)
50. K. Bolton, E. Johansson, L. Jönsson, P. Ahlström, Mol. Simulat. **35**, 888 (2009)
51. H. Docherty, A. Galindo, C. Vega, E. Sanz, J. Chem. Phys. **125**, 074510 (2006)
52. S. Moodley, E. Johansson, K. Bolton, D. Ramjugernath, Mol. Simulat. **38**, 838 (2012)
53. H.A. Lorentz, Ann. Phys. **12**, 127 (1881)
54. D.C. Berthelot, Compt. Rend. **126**, 1703 (1898)
55. T.M. Reed III, J. Phys. Chem. **59**, 425 (1955)
56. G.H. Hudson, J.C. McCoubrey, Trans. Faraday Soc. **56**, 761 (1960)
57. N.I. Papadimitriou, I.N. Tsimpanogiannis, I.G. Economou, A.K. Stubos, Mol. Phys. **112**, 2258 (2014)
58. D.E. Cristancho, I.D. Mantilla, S. Ejaz, K.R. Hall, J. Chem. Eng. Data **55**, 826 (2010)
59. I. Langmuir, J. Am. Chem. Soc. **38**, 2221 (1916)
60. J.C. Lagarias, J.A. Reeds, M.H. Wright, P.E. Wright, SIAM J. Optim. **9**, 112 (1998)